Water Air Soil Pollut (2019) 230:307
https://doi.org/10.1007/s11270-019-4363-y

Sulfur and Nitrogen Gases in the Vapor Streams from Ore Cyanidation Wastes at a Sharply Continental Climate, Western Siberia, Russia

Nataliya Yurkevich · Svetlana Bortnikova · Natalya Abrosimova · Alexei Makas · Vladimir Olenchenko · Nikolay Yurkevich · Alexey Edelev · Olga Saeva · Artem Shevko

Received: 14 September 2019 / Accepted: 5 December 2019
© Springer Nature Switzerland AG 2019

Abstract The article presents the results of the study of the vapor streams from sulfide-containing tailings after gold mining by cyanidation (Ursk waste heaps, Kemerovo region, Russia). The gas survey of sulfur dioxide, dimethyl sulfide, dimethyl sulfoxide, carbon disulfide, and N-containing substances concentrations was carried out using a portable device GANK-4 on a series of profiles covering the waste heaps and the surrounding area with simultaneous measurement of temperatures in the air and soil. The concentration maps-schemes of the studied gases in the surface layer were constructed. The high positive correlation of gases between themselves is established, which indicates similar mechanisms of their formation. The electrical resistivity tomography determined the internal structure of the waste heap. Active "breathing" zones were identified in which the maximum fluctuations in the concentrations of sulfur, selenium, and nitrogen-containing compounds in the near-surface air layer were recorded. Such zones are marked with lower resistances in comparison with other areas on the geo-electric profiles. There is an inverse correlation between the resistivity of the tailings and its temperature and a direct correlation between the concentration of gas in the air and the temperature of the soil. High concentrations of CS_2, the volatile gas compound of the second hazard class, were found in the concentrations that exceed 6–8 times the daily average norm. Further investigation of the mine tailings seasonal

N. Yurkevich · S. Bortnikova · N. Abrosimova · A. Makas · V. Olenchenko · N. Yurkevich · A. Edelev · O. Saeva
Trofimuk Institute of Petroleum Geology and Geophysics, Siberian Branch of the Russian Academy of Sciences, Koptug ave. 3, Novosibirsk, Russia 630090

S. Bortnikova
e-mail: BortnikovaSB@ipgg.sbras.ru

N. Abrosimova
e-mail: AbrosimovaNA@ipgg.sbras.ru

A. Makas
e-mail: MakasAL@ipgg.sbras.ru

V. Olenchenko
e-mail: OlenchenkoVV@ipgg.sbras.r

N. Yurkevich
e-mail: YurkevichNV2@ipgg.sbras.ru

A. Edelev
e-mail: EdelevAV@ipgg.sbras.ru

O. Saeva
e-mail: SaevaOP@ipgg.sbras.ru

N. Yurkevich
Novosibirsk State University, Pirogova str. 2, Novosibirsk, Russia 630090

N. Yurkevich (✉)
Novosibirsk State Technical University, K. Marksa ave. 20, Novosibirsk, Russia 630073
e-mail: YurkevichNV@ipgg.sbras.ru

A. Shevko
Sobolev Institute of Geology and Mineralogy SB RAS, Koptug ave. 3, Novosibirsk, Russia 630090
e-mail: sp@igm.nsc.ru

Published online: 13 December 2019

transformation with the production of toxic gases deserves special attention due to high environmental risks and poor knowledge of this problem. The oxidation of ore cyanidation wastes in summer and methylation in winter due to seasonal temperature fluctuation lead to production of gases of great concern including toxic CS_2.

Keywords Waste heap · Gas-vapor streams · Organic gases · Channels of infiltration · Micro-electrical resistivity tomography

1 Introduction

Sulfide-containing mine waste is a source of acidic drainage flows and gas emanations (Bortnikova et al. 2018). Of particular interest are seasonal variations in the structure and composition of man-made systems, depending on environmental parameters in areas with a continental climate characterized by long cold winters and short warm summers. Soils in the frozen state are a complex multiphase system, which is due to the fact that variability of temperature and pressure is continuous in the dynamics. At negative temperatures, the electric potential jumps at the film-ice boundary and the rates of some chemical reactions increase (Pticyn 2006). The most intensive geochemical transformations are subjected to a layer of seasonal temperature fluctuations, in which chemical leaching is activated, associated with rock cracking under the influence of expanding and freezing pore fluid. The sulfide-bearing rock is exposed in such conditions the oxidation of the formed acidic drainage, leached metals, and metalloids (Yurkevich et al. 2017a). In addition, a whole range of sulfur and selenium-containing gases, including those of organic origin, are released from sulfide-containing waste, metals, and metalloids that are found in the air above the surface of the dumps, as we wrote in works (Bortnikova et al. 2017, 2018, 2019). However, the mechanisms, as well as the toxicity of the detected gases, remain poorly understood.

The discovery of substantial amounts of volatile organo sulfides was first revealed in the oceans and became one of the major additions to the sulfur cycle in the second half of the twentieth century. *Dimethyl sulfide* (DMS) represents a major flux of sulfur to the atmosphere (Bates et al. 1992; Brimblecombe 2013; Gourdal et al. 2018), plays a globally significant role in carbon and sulfur cycling, and affects the Earth's climate because its oxidation products serve as nuclei to form clouds (Koch and Dahl 2018). DMS is also a climate-relevant gas potentially involved in a feedback loop known as the CLAW hypothesis (Charlson et al. 1987). The production of DMS is driven by the activity of microbiological organisms (Kiene et al. 2000).

DMS stems mainly from the enzymatic cleavage of dimethylsulfoniopropionate (DMSP) by algal and bacterial DMSP lyases in ocean water. DMSP dissolved in water is then readily available to heterotrophic bacteria as carbon and sulfur sources (Kiene 1990; Kiene et al. 2000; Simó 2001; Vila-Costa et al. 2006; Gourdal et al. 2018; Ledyard & Dacey 1996; Malin & Kirst 1997). DMS revealed in the air above burning coal mine heaps (BCMH) (Kruszewski et al. 2018), during reductive soil disinfestation sulfate (SO_4^{2-}) transformation (Meng et al. 2015), reduction of dimethylsulfoxide, methylation of sulfide or methanethiol (CH_3–SH, MT), as well as anthropogenic emissions from wastewater treatment, and other sources (Hayes et al. 2010; Carrión et al. 2017; Koch and Dahl 2018).

The presence of dimethyl sulfide in the air above the sulfide dumps is first mentioned in the paper (Bortnikova et al. 2018). The presence of dimethyl sulfide (C_2H_6S), in our opinion, indicates methylation of sulfide-containing compounds by autotrophic microorganisms *Pseudomonas* sp. and *Bacillus* sp. (we found earlier in this waste) by the reaction:

$$S2^- + 2\ CH3 + \rightarrow \qquad (C2H6S.C2H6S.)$$

The dimethyl sulfide molecule has a dipole moment (1.51 g) comparable to that of a water molecule (1.84 g), which indicates a high probability of formation of polar ion bonds of DMS with divalent metal cations and their involvement in gas transport (Bortnikova et al. 2018).

Dimethyl sulfoxide (DMSO) is a product of the oxidation of dimethyl sulfide. More and more evidence suggests that particulate matter DMSP (DMSP) may be involved in osmoprotection, cryoprotection (Lee and de Mora 1999), and antioxidant defense mechanisms (Sunda et al. 2002; Gourdal et al. 2018).

Carbon disulfide (CS_2) is the metastable product of sulfide mineral oxidation (Hale 2010). Previous investigations of mineral deposits and mine tailings have led to the conclusion that CS_2 soil anomalies occur over mineral deposits where pyrite is an accessory mineral that is not directly associated with the mineralization

(Bortnikova et al. 2018). In fact, CS_2 is one of the least soluble of the sulfur gases, which may be a significant factor for their detection in the gas phase over mineral deposits experiencing oxidation under moist or saturated conditions. In addition, CS_2 is one of the most stable in air, which favors their persistence during gas-phase dispersion through permeable rocks and overburden (Hale 1993).

Sulfur oxide (IV) is an intermediate product of the oxidation of sulfide minerals. Due to its high volatility, it produces reaction zones. The main reasons for the changes in SO_2 content observed over time are probably the daily temperature fluctuations and different cooling patterns of solid materials and air. The latter reason not only leads to gas emissions from interporous space but also changes the activity of the bacterial communities that are transforming the mineral matrix of tailings. Spatial fluctuations in emissions of SO_2 can be associated with variations in humidity and the permeability of the waste (Hale 1993, 2010), but are mainly due to the heterogeneous composition of the material, namely, differences in the contents of sulfides (Bortnikova et al. 2018). The presence at North Silver Bell of anomalies of SO_2, which are more restricted in areal extent than those of CS_2 but reach peak values of more than 300 ppb over the orebody, is attributed to the shallowness of the ore deposit and the hot, dry environment. In the usually moist soils over mineral deposits in western Europe, Nicholson et al. (1988) found no SO_2 (Hale 1993). SO_2, CS_2, DMS found in the air above burning coal mine heaps (BCMH) of Upper Silesian Coal Basin (Kruszewski et al. 2018).

These substances in a vapor streams are products of reduction and oxidation processes occurring in the dumps under the influence of biotic and inorganic factors and are integral parts of the cycle of sulfur, selenium, nitrogen in the "waste-air". Understanding the laws of this cycle is necessary to establish the mechanisms of migration of chemical elements in technogenic hypergenic conditions at phase transitions between solid and gas.

One of the methods of monitoring gas emission in the near-surface space is electrical resistivity tomography (ERT). Time-lapse geophysical investigations allow to define the water flow and solute dynamics (Busato et al. 2019; Binley et al. 2015; Guerin 2005; Jougnot et al 2018). Geophysical observations of CH_4 biogenic methane emissions from peatlands indicate that gas emissions are related to changes in atmospheric pressure, precipitation, and saturation of the vadose zone (Terry et al. 2016). The role of these dynamic parameters in the evolution of gas plumes, as well as their relationship with variations in physical and geochemical parameters (e.g., permeability, capillary effect, solubility, and diffusion of gas) of the aquifer are considered in the paper (Cahill et al. 2017), but not yet sufficiently studied. However, the results of geophysical monitoring of oil wells (Steelman et al. 2017) show that ERT can be used to monitor CH_4 leaks into deeper aquifers: the variation in dissolved gas pressure has a direct correlation with the electrical resistivity (ER) of the medium. The ERT method has been successfully applied by numerous authors to detect CO_2 in water-saturated geological environments (Xue et al. 2006; Auken et al. 2014; Bergmann et al. 2017; Kremer et al. 2018). In another previous work, Kremer et al. (2018) experimentally simulated circulation of reactive CO_2 gas and inert N_2 in two types of soils: carbonate and siliceous. The results showed that the ERT method can be used to contour the plumes of gas circulation. The increase in the resistivity of the medium is due to the penetration of the gas-insulator into the porous space, the decrease in ER is due to the dissolution processes that increase the concentration of ions in the saturating pore fluid. In another study (Golebiowski et al. 2018), it was revealed that ERT surveys can be effectively applied in mining conditions to detect the fractured zones which might be sources of outflow of gas and/or water to the excavations.

In other works of previous years, the authors showed that the processes occurring in the dumps, including oxidation, formation, and migration of pore solutions, can be studied using the ERT (Olenchenko et al. 2016; Yurkevich et al. 2017a, b; Epov et al. 2017), including the application of the method to waste heaps of metallurgical slags after combustion showed that the local anomaly of extremely low resistivity (0.3–0.5 Ohm·m) might be associated with a combustion center, which are zones of active emission of gases and transfer of chemical elements in the gas phase (Bortnikova et al. 2017).

As the result of the previous investigations on gas emanations, we evaluated the possible sources and mechanisms of chemical element, including metals, transport by low-temperature gas flows (Bortnikova et al. 2018, 2019), the composition of gases, and trace contaminants in the air over sulfide waste heap (Bortnikova et al. 2017, 2019). The main attention in these works was paid to the main sources and mechanisms of metal entry into the gas phase based on an

analysis of the compositions of solids, pore solutions, secondary mineral phases, and gas condensates. In 2017, gases of presumably biotic origin were discovered for the first time by portable gas analyzer, and assumptions were made about the mechanism of throwing, which leads to the appearance of the dimethyl sulfide and dimethylselenide in the air. In this study, quantitative estimation of the gas concentrations was made. However, no quantitative estimates were made and no mechanisms for the formation of such emanations were established.

Recent studies have shown that dynamic observations of the system make it possible to identify areas of active hypergenic transformations, including those with gas emanations (Osipova et al. 2018). In addition, it was found that the electrical resistivity of the soil is closely related to the temperature of the air, which in turn affects the emanation of gases. Therefore, it seems promising to use methods of electrical prospecting for a better understanding of the processes occurring in such systems. The purpose of this work was to determine the composition of and quantitative estimation of the gas flows from the surface of the tailings and in the surrounding area with the establishment of possible sources of anomalies in the air, interrelations of geoelectric (ER), geochemical parameters of the technogenic environment, and external environmental parameters (air temperature) in winter and summer on the example of the Ursk waste heap of the gold deposit (Kemerovo region).

2 Study Area

The Ursk waste heaps are located in the village Ursk (Kemerovo region, Salair Ridge). The heaps originated in the 1930s and stored the wastes of the cyanidation of the weathering ores of the Novo-Ursk deposit. The upper parts of the ore bodies (loose quartz-barite and quartz-pyrite material) were mined, and gold was extracted by cyanidation (Fig. 1). Processed ore waste was stored as heaps. A natural stream flows near its foot, becoming an acidic, highly mineralized stream after the heap.

The Novo-Ursk deposit was discovered in 1932 as a part of the Ursk ore field, which combines the Novo-Ursk, Beloklyuch, Samoilov deposits and a number of ore occurrences. The structure, morphology, and composition of the ore bodies, the sequence of mineral formation, and the history of mining have been studied and described by many researchers; thus, a brief description of the ore field is given in these papers (Bolgov 1937; Zerkalov 1959; Kovalev 1969; Distanov 1977). The main sulfide minerals in the ores of the Ursk field are pyrite, arsenopyrite, sphalerite, chalcopyrite, tetrahedrite, and galena. The vein minerals present are quartz, sericite, barite, calcite, and gypsum. Following the discovery, the mining of the oxidation zone of the Novo-Ursk deposit began.

From the surface, it was represented by a typical gossan with a high content of barite and gold. At the deposit, oxidized ore bodies were extracted to a depth of 40–50 m. Only the upper part of the ore bodies was worked out: a quartz-baritic loose sand (the most oxidized part of the ore bodies) and a quartz-pyrite (a less oxidized substance), from which gold was extracted by cyanidation. Wastes were stored side by side in the floodplain of the stream in two waste heaps without protective technical structures or dams. As a result, heaps 10–12 m high were formed (Yurkevich et al. 2017a). The quartz-pyrite waste heap has been largely removed in the last decade for secondary extraction of barite. The second, from the waste of the oxidation zone, remained unchanged.

A comprehensive geophysical and geochemical study of the acid drainage distribution area in the vicinity of the investigated heaps in past research allowed us to determine two migration directions of highly mineralized toxic solutions. Surface runoff is on the natural slope of the valley, in the vertical direction along the natural fracture, drainage flows penetrate into the groundwater to a depth of more than 20 m (Olenchenko et al. 2016).

3 Methods

3.1 Field Measurements

3.1.1 Vapor Phase Composition

The composition of volatile compounds produced by the material dumps was studied in 2016–2018 by several methods.

Gas surveys at the dumps and the adjacent territory were carried out using a GANK-4 portable gas analyzer (NPO GANK, Moscow) (manufactured by "NPO PRIOR GANK", Russia) (Bortnikova et al. 2018) at 30 points through 20 m. The gas analyzer GANK-4 is

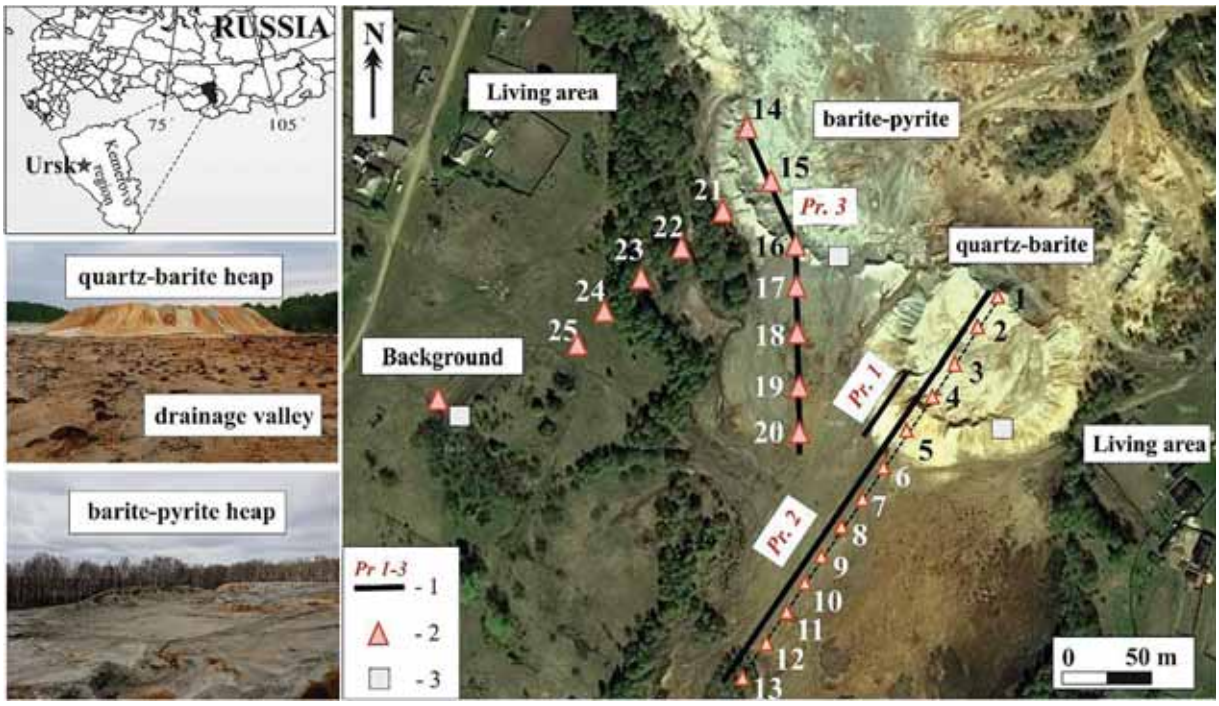

Fig. 1 Location and photos of quartz-barite and barite-pyrite Ursk waste heaps, study scheme on the Ursk heap: (1) profiles of ERT, (2) points for measuring of DMS, DMSO, CS2, SO2 concentrations and soil temperature, (3) pits

intended for automatic continuous or periodic control of 25 harmful substance concentrations in one device without sample preparation in atmospheric air. It includes the electrochemical, thermocatalytic, and semiconductor built-in sensors, the replaceable chemical cartridge, the afterburner, and chemical cartridges. The limit of the main relative error is ± 20%, the limit of the allowed additional error is no more than 0.6 (from the main), the air consumption with the chemical cartridge 0.5 ± 0.1 l/min, the air consumption on sensors 1.8 ± 0.2 l/min (https://gank4.all.biz/en).

The measurements were carried out on four profiles: 13 points on the quartz-barite dump and in the SW direction from it in the drainage valley (red triangles, points 1–13; Fig. 1), seven points on the barite-pyrite dump and to the south (red triangles, points 14–20; Fig. 1), five points in the forest zone in the SW direction from the pyrite heap (red triangles, points 21–25; Fig. 1), as well as in the background point in the forest zone (background; Fig. 1). Concentrations of DMS (dimethyl sulfide C_2H_6S), DMSO (dimethyl sulfoxide C_2H_6SO), carbon disulfide (CS_2), sulfur dioxide SO_2 in atmospheric air above the earth's surface were determined in a windless solar time in the period from 12.00 to 18.00. The gas analyzer tube was kept at a distance of 10 cm from the surface of the soil, and three parallel readings were recorded with subsequent averaging.

1. For qualitative analyses of mine tailings's vapor, emanation air was sampled on-site on concentrators by sampling pump ANP-11 (SIBEL Ltd., Novosibirsk). Then, samples were delivered to the laboratory and analyzed by gas chromatography/mass spectrometry method (GC/MS).
2. On February 2018, at the sites with a contrasting distribution of gases, gas concentrations in the near-surface air layer under the snow cover were measured. On a profile, 14 m long, a snow layer on the slope was removed, and the gases were measured in the same way as in summer. At the same points, the temperature of the soil was measured using a thermal probe at a depth of 0.1 m. The concentrations of gases in May were determined on the same microprofile.

3.1.2 Electrical Resistivity Tomography

Geoelectric sections were constructed using an electrical resistivity tomography (ERT) method to

determine the internal structure of the near-surface space at the same profiles as for gas survey. Profile 1—on the slope of a quartz-barite dump of southern exposure, 14 m length, step between measurements 30 cm (Fig. 1, Pr1). Profile 2 crosses the quartz-barite heap, a talus fan and a drainage valley in the south-western direction, 240 m length, distance between electrodes—5 m, with a starting point on the surface of the heap, and with the end in the grove on the border with the drainage valley (Fig. 1, Pr2). Profile 3 with a length of 120 m and step between the electrodes of 5 m starts at the top of the pyrite dump and lays along its southern slope and the drainage valley in a southern direction (Fig. 1, Pr3). The measurements were carried out using the multielectrode resistivity meter "SKALA-48" (Skala-48, IPGG SB RAS, Novosibirsk, Russia). ERT was performed using a Schlumberger array.

A plot with contrasting concentrations of gases (the slope of the southern exposure of the barite dump) was selected for monitoring observations by micro-electrotomography. Measurements were made in summer and winter in this profile, with simultaneous measurement of gas concentrations. Within the study site, micro-soundings were made on the profile along the slope (Fig. 1) to study the detailed structure of the upper part of the section to a depth of 3 m in winter (February) and spring (May) time. The sequence of connecting the electrodes corresponded to a dipole-axial installation with a maximum spacing of the centers of the supply and receiving dipoles of 5.25 m. Data processing was performed using Res2Dinv software (Loke 2000). Two-dimensional geoelectric sections of the resistivity distribution in the area were constructed using the results of data processing.

3.1.3 Solid Matter Sampling

The materials in the dump were sampled from the test pits with a depth of 20 cm with a plastic sampler. The samples were divided into two parts and packed in sealed plastic bags. One part of the sample was intended to determine the chemical composition, the second was to extract the pore water, from the third part of the sample, water-soluble compounds were extracted in the laboratory.

3.2 Laboratory Analysis

3.2.1 Sample Preparation

Pore solutions were squeezed from the first of the two parallel samples at a pressure of 100 Pa according to (BS ISO 1998). The second set (10 g) was dried at room temperature for 48 h, homogenized, and powdered to < 74 μm by abrasion in an agate mortar for bulk analysis. From the third part of the sample, water-soluble species were extracted.

3.2.2 Analysis of Solid Samples for Trace and Major Elements and Mineral Composition

The contents of major oxides in the bulk solid samples were determined via X-ray fluorescence analysis from a 3-g sample aliquot. The elemental composition of solid material was determined using inductively coupled plasma atomic mass spectrometry ELAN-9000 DRC-e, Perkin Elmer, USA ("PLASMA" Company, Tomsk).

Morphology and composition of mine tailings were identified using scanning electron microscopy (SEM) TESCAN MIRA3 LMU (Czech Republic) with an INCA Energy 450+ microanalyzer based on the Oxford Instruments NanoAnalysis X-MAX 80 (UK) system (laboratory of X-ray spectral analysis methods of the Institute of Geology and Mineralogy, Novosibirsk).

3.2.3 Gas Chromato-Mass Spectrometry

Qualitative analyses of the vapor phase from waste samples were carried out using a field gas chromatograph/mass spectrometer MCMS "NAVAL" (SIBEL Ltd., Novosibirsk) previously developed at the Laboratory of Field Analytical and Measurement Technologies of IPGG SB RAS (Makas and Troshkov 2004). The sampled air was pumped through concentrators comprising thin-walled stainless steel tubes with an outer diameter of 2 mm containing a layer of Tenax TA sorbent (10 mg). The sample was introduced into the GC column by direct flash thermal desorption in a stream of helium at a temperature of 300 °C. The parameters of the GC column are 0.32 mm × 1 μm × 15 m (HP-5MS, Agilent Technologies, USA). The GC separation mode involved holding the temperature at 90 °C for 3 min then increasing it to 250 °C at a rate of 10 °C/min. The resulting GC/MS data were processed using the AMDIS (AutomaticMass Spectral Deconvolution

and Identification System) program, and the identification of individual components was performed using the mass spectra of electron ionization using the NIST/EPA/NIH mass spectral library (edition 2017).

4 Results and Discussion

4.1 Chemical and Mineralogical Composition of the Ursk Wastes

At the surface, the oxidized quartz-barite heap is represented by a loose, dry large-medium-grained material of predominantly bright red and brick color, with inclusions of gravel and crushed stone.

The less oxidized barite-pyrite dump is composed of medium-fine-grained gray sand, on the surface is covered with white and light yellow efflorescence, and alternates with layers of blue-green and blue at a depth of 20–70 cm. If we consider a substance stored in a quartz-barite heap as a result of oxidative weathering and leaching of pyrite material, then a comparison of their microelement compositions may indicate the processes of fractionation of chemical elements in the process of hypergenesis.

The composition of the dumps differs both in the content of oxides of the silicate group and in the trace element composition (Table 1). The substance of the quartz-barite dump contains a larger amount of rock-forming elements, and the substance of the barite-pyrite dump contains iron and sulfide sulfur (due to pyrite).

In the mineral composition, barite heap also differs from pyrite heap; barite and pyrite with inclusions of various sulfides and sulfates are determined as part of the pyrite dump: tennantite with Se (up to 0.055 wt%), Sb (up to 2.75 wt%), Zn (up to 3.05 wt%) impurities (Fig. 2b, e), chalcopyrite (Fig. 2a, b), Cu-Fe-S sulfide containing Se (up to 0.33 wt%), Sb (up to 2.1 wt%), As (up to 4.7 wt%), Te (up to 12 wt%), Zn (up to 0.03 wt%) (Fig. 2a), anglesite (Fig. 2c), galena with Te (up to 0.072 wt%), and Sb (up to 0.08 wt%) (Fig. 2d). The mineral composition of the barite heap is dominated by barite with single grains of pyrite.

4.2 Composition of the Vapor-Gas Phase

Dimethyl sulfide (DMS), dimethyl sulfoxide (DMSO), sulfur dioxide (SO_2), and carbon disulfide (CS_2) were detected using GANK-4 portable gas analyzer at all points of the profiles in the surface air layer (Fig. 3). The highest concentrations of all gases were found at the points of Pr2, crossing the quartz-barite dump along with the talus fan down to the valley. The concentration of SO_2 significantly exceeds the concentration of the measured gases: its content varies from 140 to 3600 μg/m^3, in five points of the profile it exceeds the maximum allowable concentration (MAC). The highest contrast distribution of gases was found on the same profile. The maximum concentration of gases is confined to the point #5, located at the foot of the dump, and then, they decrease along the profile, but remain higher than at points on the dump.

From the profile of the pyrite heap (points 14–20; Fig. 3), the opposite trend is observed. The content of sulfur dioxide, which is relatively high above the top of the heap (160–330 μg/m^3), sharply decreases at its foothills and on the valley (23–73 μg/m^3). The same, but less contrasting trend is observed for other gases. In addition, dimethyl selenide C_2H_6Se was detected at points on the pyrite profile according to GC-MS. In general, a high positive correlation had been established between gas concentrations, which may be a consequence of a similar mechanism of their formation during interactions of biotic and inorganic components (Table 2).

Note that in most points, the concentration of the DMSO and sulfur dioxide exceeds the concentration of DMS and carbon disulfide. This indicates a greater intensity of oxidation reactions than the reductive.

4.3 Geoelectrical Zonality of the Heaps

4.3.1 Quartz-Barite Heap

The body of the heap is composed of a non-uniform material, which is reflected in variations of the electrical resistivity in a wide range from 1 to 350 Ohm·m. Low-resistance areas are localized at depths of 2.5–7 m from the surface at the pickets of 10–20, 35–50, and 55–60 m along the profile (Fig. 4a).

The surface of the heap to a depth of 1 m in the initial marks of the profile to a depth of 6 m at the pickets of 30 m and 60 m is composed of loose dry rocks with a resistance of 30–150 Ohm·m. The nature of the location of contrasting resistivity rocks indicates the infiltration of acidic drainage from the surface into the dump with oxidation, weathering, and loosening of the original

Table 1 Composition of the solid matter in the Ursk waste heaps. Note: n.d. no data; "*" after (Lazareva et al. 2019)

	Oxidized quartz-barite heap (QB)				Less oxidized barite- pyrite heap (BP)			
	Mean	Min	Max	St. dev.	Mean	Min	Max	St. dev.
%, $n = 20$								
SiO_2	63.74	61.35	66.32	2.29	28.02	20.86	33.42	6.5
TiO_2	0.77	0.61	0.96	0.15	0.36	0.25	0.44	0.1
Al_2O_3	2.81	2.36	3.09	0.31	0.93	0.66	1.23	0.3
Fe_2O_3	4.49	3.47	4.91	0.68	25.50	21.22	30.74	4.8
MnO	0.01	0.00	0.02	0.01	0.00	0.00	0.01	0.0
MgO	0.06	0.04	0.08	0.02	0.02	0.02	0.02	0.0
CaO	0.27	0.04	0.55	0.21	0.12	0.09	0.15	0.0
Na_2O	0.26	0.19	0.28	0.04	0.11	0.08	0.12	0.0
K_2O	0.82	0.69	1.00	0.13	0.32	0.20	0.39	0.1
BaO	15.06	13.67	15.75	0.94	16.02	14.91	17.45	1.3
$S_{sulfate}$	0.70	0.46	0.92	0.19	0.78	0.71	0.88	0.1
$S_{sulfide}$	2.54	2.47	2.59	0.05	21.1	18.8	23.9	2.6
%, $n = 3$								
N*	< 0.05			n.d.	< 0.05			n.d.
C*	0.3	0.025	0.9	0.5	0.03	0.025	0.05	0.014
H*	0.4	0.3	0.6	0.15	0.2	0.05	0.4	0.18
ppm, $n = 20$								
Cu	47	40	60	9.1	514	425	629	105
Zn	36	32	41	3.5	94	77	120	23
Pb	2750	2400	3000	265	1667	1600	1800	115
Cd	0.38	0.35	0.40	0.02	0.37	0.34	0.40	0.0
Cr	34	26	42	6.5	24	14	38	12
Co	0.57	0.43	0.69	0.12	4.51	2.45	7.14	2.4
As	440	422	452	14	658	640	684	23
Sb	561	516	612	44	222	118	323	103
Ag	29	25	31	3.0	23	17	30	6.6
Mo	8.8	8.2	10	0.79	15	14	18	2.4
Sn	4.7	4.4	5.0	0.24	1.94	1.50	2.4	0.5
Rb	9.0	7.6	11	1.4	3.6	3.0	4.6	0.8
Sr	528	513	560	22	227	210	237	15
V	27	2	96	35	9.2	5.0	13	3.3
Cs	0.45	0.43	0.49	0.029	0.22	0.19	0.27	0.044

waste material. It can be assumed that there are filtering channels at 55 and 65 m along the profile (Fig. 4a).

The slope of the heap is represented by rocks with resistivities of 30–65 Ohm·m over the entire depth of sounding. Rocks here are subject to intensive weathering and freezing. At the foothills of the heap at pickets of 80–95 m, a low-resistivity anomaly (1–5 Ohm·m) with a capacity of 2.5 m is observed at a depth of 1–5 m. After a mark of 95 m, this anomaly reaches the surface and extends to 190 m and is confined to the soils of a valley formed due to the migration of drainage flows and the removal of the clay part of the waste from dumps. At the base of the technogenic soils are high-resistance soils of the natural log. Toward the end of the profile, the layer of wastes becomes thinner up to a thickness of 1 m at a mark of 240 m.

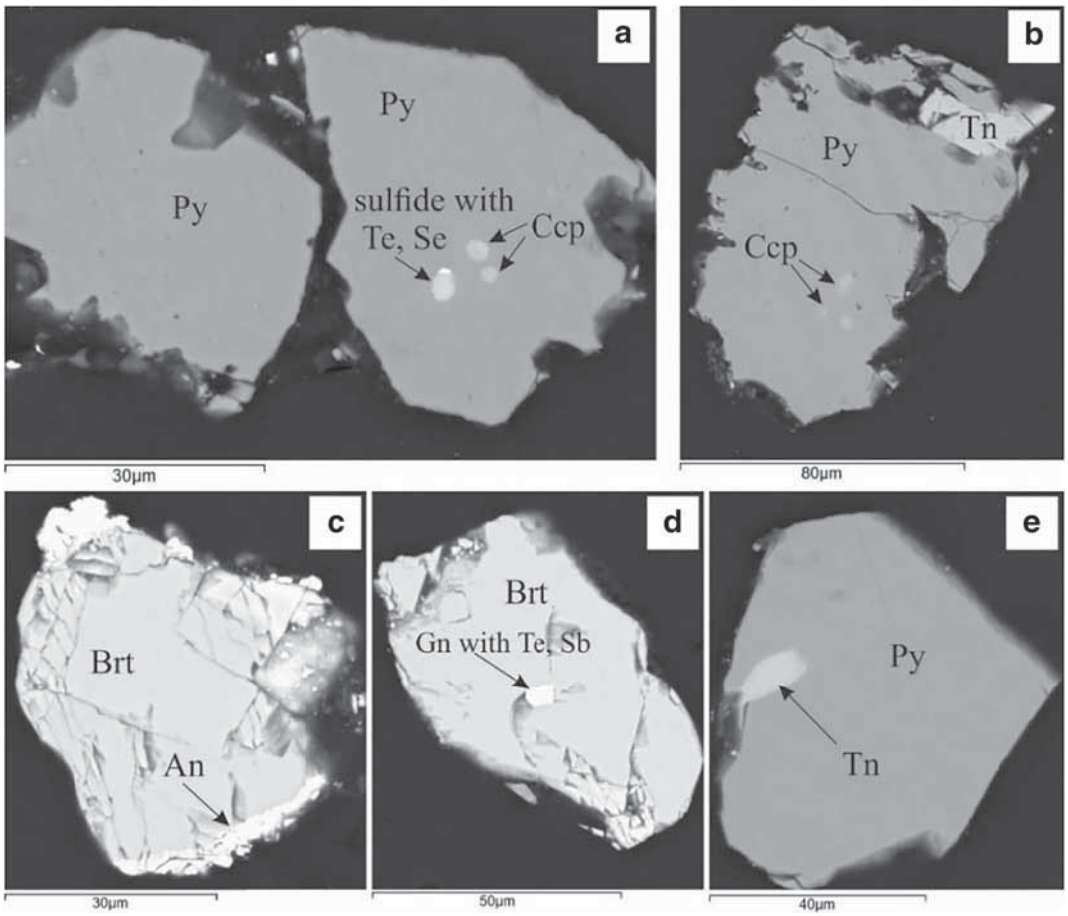

Fig. 2 SEM images of the minerals detected in the tailings of the barite-pyrite heap: pyrite (Py) with inclusions of Se and Te sulfides and chalcopyrite (Ccp) (**a**), chalcopyrite (Ccp) and tennantite (Tn) (**b**, **e**); grains of barite (Brt) intergrown with anglesite (An) (**c**), and with inclusion of galena (Gn) (**d**)

A detailed study of the geoelectric zonality was carried out on the site with abnormal gas concentrations. Electrical resistivity tomography micro-profiles (micro-ERT) were built on the slope of the quartz-barite heap (Fig. 4b). The values of the resistivity in the subsurface space on the slope and at the foot vary in the range of 1–200 Ohm·m, but there is a zone of low resistivity under the foot at a depth of 0.5–1.5 m, which probably corresponds to a lens with highly mineralized porous solutions. The location of the exit channel of infiltration solutions to the surface corresponds to the zone with abnormal gas concentrations. The presence of areas enriched with a heavy fraction (sulfide material) in combination with highly mineralized acid solutions coming from below promotes decomposition reactions of sulfides with the production of sulfur gases and the more intensive removal of chemical elements than at the top of the dump.

4.3.2 Winter Observations (February)

Measurements on the same micro-profile 1 were repeated in winter time (February) with simultaneous measurement of gas concentrations at its points.

The upper part of the geoelectrical section along with the Pr1 microtomography profile (Fig. 4c) to a depth of 0.65 m was characterized by high resistivity (500–10,000 Ohm·m), which was associated with seasonal freezing. There was no snow on the slope of the dump, and the freezing was relatively deep. In the interval of the profile of 9.5–11.5 m, an anomaly reduced to 50 Ohm·m resistivity is distinguished. At this point, the incision was blocked by a layer of snow 0.5 m thick, which prevented freezing. The configuration of the lens of highly mineralized pore water at the base of the incision remains the same as in summer.

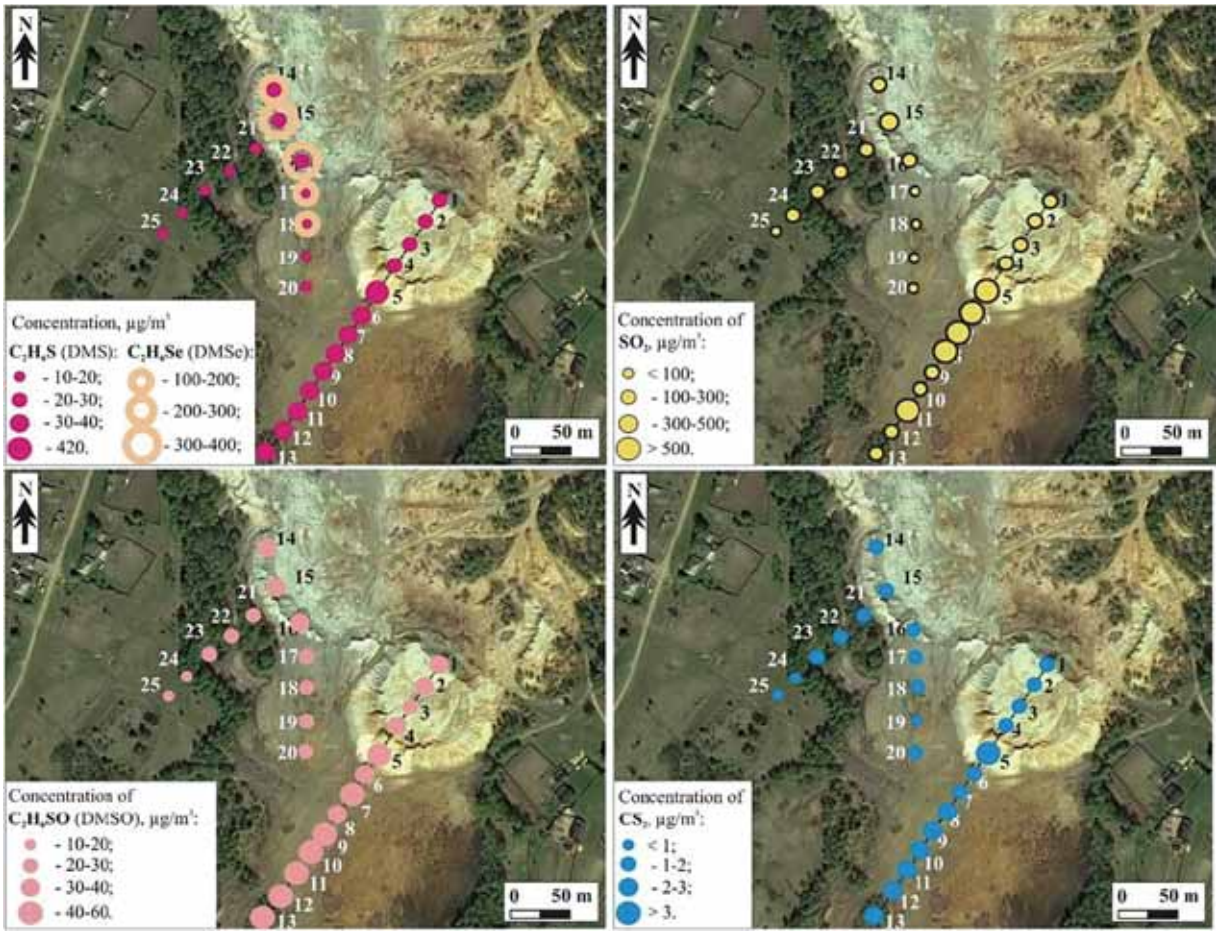

Fig. 3 Concentrations of dimethyl sulfide, dimethyl selenide, sulfur dioxide, dimethyl sulphoxide, and carbon disulfide in the near-surface layer according to GANK-4 and GC-MS measurements

Comparison of the geoelectric profile with temperature data shows that the local anomaly of lowered electrical resistivity in the range of 9.5–11.5 m has the positive soil temperature (+ 0.4 °C), while in the rest of the profile, it is negative (− 5 °C; Fig. 4c).

Above the same ER anomaly, there is an increased concentration of DMS in the surface layer (up to 0.2 mg/m^3) relative to the MPC (0.08 mg/m^3). At other sampling points, where the upper part of the section is marked by high resistivity, the concentration of LCA does not exceed 0.04 mg/m^3 (Fig. 5).

Table 2 Correlation coefficients of the DMS, DMSO, CS_2, SO_2 concentrations

	DMS	DMSO	CS_2
DMSO	0.61		
CS_2	0.73	0.72	
SO_2	0.83	0.66	0.72

An analysis of the soil temperature, DMS and resistivity concentrations at a depth of 0.1 m (Fig. 5) show that there is a close relationship between these parameters. There are low resistivity and high DMS concentrations in the area of positive temperatures. However, at a point of 12.3 m of the section, high ER is associated with the dry state of rocks at positive temperatures. Low humidity causes low activity of methylation processes and the formation of DMS.

Seasonal observations on quartz-barite dumps showed that the temperature of soils in June rose by 10–15 °C compared to May parameters, but it is distributed less evenly. At the pickets of 80 and 240 m, minima are observed, and at 100 m, a maximum is observed in the results of both May and June measurements.

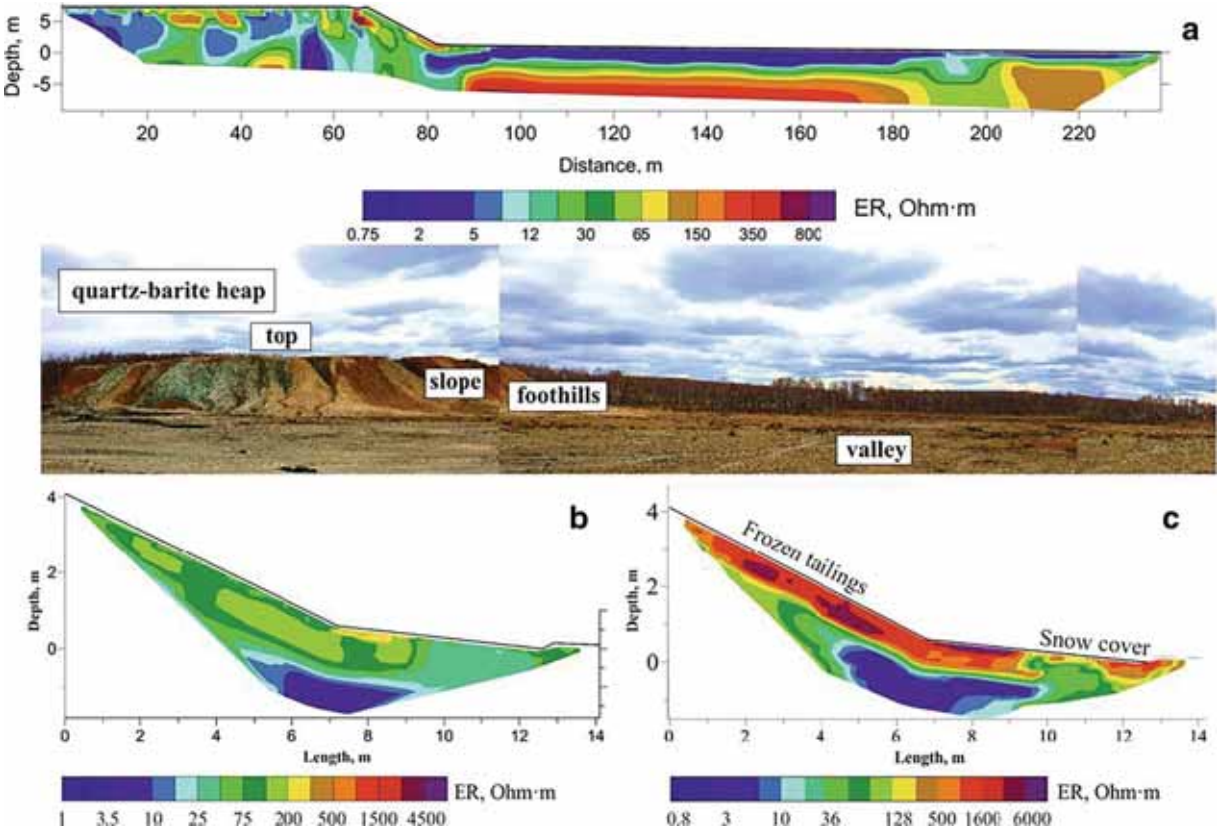

Fig. 4 Geo-electric sections: **a** along the Pr2 profile of the quartz-barite heap, a photo with a general view of the heap and drainage valley. The micro-profile 1 area is highlighted in the black rectangle (see Fig. 1). **b** Geoelectrical section of the slope of the quartz-barite heap on the micro-profile 1 in the spring time. **c** Geoelectrical section of the slope of the quartz-barite heap on micro-profile 1 in the winter time

This zone (80–100 m in profile) corresponds to the basset of the low-resistance anomaly on the surface of the heap, which we noted above. The DMS and DMSO concentration discontinuities are noted at this point. Apparently, a geochemical barrier is formed in this area due to a change in physicochemical conditions when

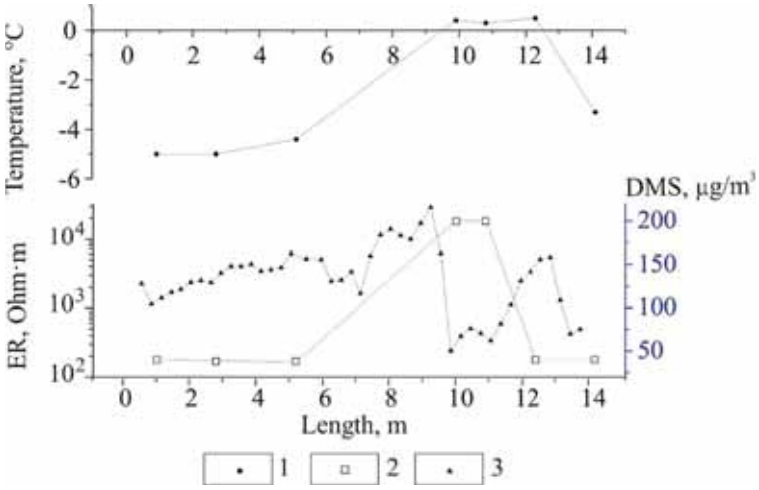

Fig. 5 Temperature (Auken et al. 2014), DMS concentration (Bates et al. 1992), и electrical resistivity (Beloborodova and Beloborodov 2000) on the depth of 0.1 m on profile 1

acidic drainage from the oxidation zone gets into natural soils. The elevated concentrations of DMS and SO_2 at the drainage valley indicate this area as "breathing" (Fig. 1, point 5). Activity in the gas production may be associated with the development of a specific biotic community characteristic of transition zones in natural-technogenic systems.

4.4 Barite-Pyrite Heap

On the pyrite-barite heap, unlike quartz-barite, low-resistivity zones (saturated with highly mineralized pore solutions), in which there is the most intensive interaction, approach the surface at the top of the heap, and then, they are replaced by a section with lower electrical conductivity (Fig. 6).

4.5 The Composition of Air Above the Surface of Barite-Pyrite and Quartz-Barite Heaps According to Gas Chromatography–Mass Spectrometry

About 100 volatile organic compounds were identified in air samples over the heaps using GC/MS analysis. Concentrations of a number of compounds of sulfur, selenium, and nitrogen, as well as aldehydes, alcohols, and acids, significantly exceed background levels (Table 3).

As it was mentioned above, according to the portable gas survey, dimethyl sulfide, and dimethyl sulfoxide were found in the air, the concentrations of which correlate with each other, which indicates the interconnection of the processes that lead to the gases formation. We suggest that dimethyl sulfide is a biological methylation product of sulfide-containing waste components. The oxidation of the dimethyl sulfide with oxygen leads to the formation of dimethyl sulfoxide (Gourdal et al. 2018). GC-MS confirms the presence in the air of DMSO, as well as other methylated forms (containing methyl groups -CH_3) of sulfur-containing compounds: dimethyl disulfide DMDS ($C_2H_6S_2$), dimethyl trisulfide DMTS ($C_2H_6S_3$). DMDS and DMTS are volatile organic compounds with an unpleasant odor and high reactivity, which is caused by the weakness of the S–S bonds in these molecules. It is known that, for example, DMTS ($C_2H_6S_3$) is a decomposition product of bacterial decomposition (Statheropoulosa et al. 2007).

DMDS is a widespread natural odoriferous compound emitted from many sources such as plants (Stensmyr et al. 2002a), fungi (Johnson and Jürgens 2010). We assume that these compounds are metabolites of the bacterial transformation of sulfur-containing compounds in sulfide heaps, which was mentioned earlier (Bortnikova et al. 2018). Moreover, unlike our previous data on organic gases above the sulfide tailings (Bortnikova et al. 2018, 2019), in this study, quantitative estimation of the gases concentrations was made. It is noteworthy that compounds containing methyl groups are found in the air above the quartz-barite heap in higher concentration than above the barite-pyrite heap (Table 3). In addition, aromatic compounds are found over quartz-barite heap: phenol (3 μg/m^3), benzonitrile (17.2 μg/m^3), and benzamide, N, N-dimethyl- (6 μg/m^3). Notable high concentrations of nonanal ($C_9H_{18}O$) in the air above the quartz-barite (9.8 μg/m^3) and barite-pyrite (85.5 μg/m^3) heaps. Nonanal acts synergistically with carbon dioxide (Bowman et al. 2003).

The presence of carbon disulfide CS_2 in the air above the heaps was recorded earlier (Bortnikova et al. 2018, 2019). In the works of Hale (1993, 2010), data on the stability of CS_2 in the air above sulfide deposits were provided, which can be used as an indicator sign during prospecting. In the case of Ursk waste heap, both above quartz-barite and above barite-pyrite heaps, high concentrations of CS_2 were

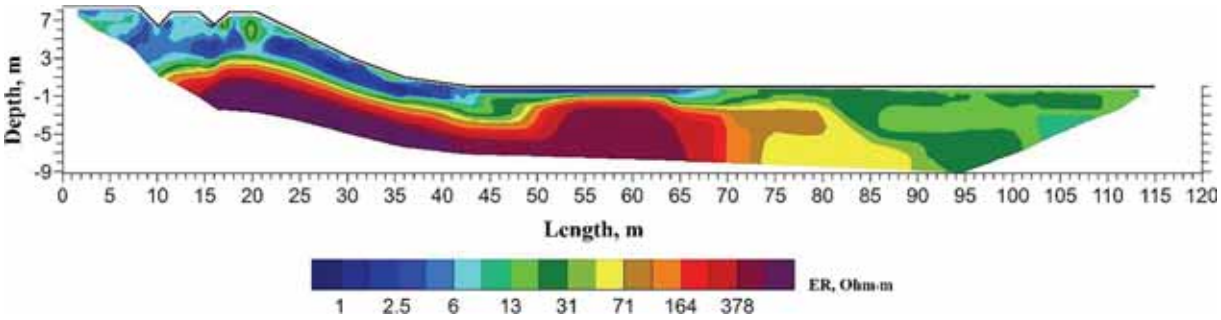

Fig. 6 Geoelectrical section of profile 3 on the pyrite-barite heap

Table 3 Concentrations of organic compounds in the air above the Ursk heaps, μg/m^3

Component	Q-B	B-P	BG	MPC (GN 2.1.6.1338–03) GN (Hygienic Norms) no. 2.1.6.1338–03. (2003)		
				msd	ad	hc
Carbon disulfide	31.0	43.4	93.0	30	5	2
Dimethyl selenide	51.8	bdl	bdl	nd	nd	nd
Disulfide, dimethyl	2.3	11.4	bdl	700	nd	4
Trisulfide, dimethyl	0.3	0.2	bdl	nd	nd	nd
Pyridine	15.0	bdl	bdl	80	nd	2
Formamide, N,N-dimethyl-	45.0	bdl	bdl	nd	30	3
N,N-dimethylacetamide	4.2	bdl	bdl	200	6	2
Benzamide, N,N-dimethyl-	6.0	bdl	bdl	75	30	3
Phenol	3.0	0.4	0.2	7	nd	3
Benzonitrile	17.2	0.2	bdl	nd	nd	nd
Benzyl nitrile	0.4	bdl	bdl	nd	nd	nd
2-Pyridinecarbonitrile	0.8	bdl	bdl	nd	nd	nd
Benzenepropanenitrile	0.2	bdl	bdl	nd	nd	nd
1,2-Benzenedicarbonitrile	1.0	bdl	bdl	nd	nd	nd
Hexanal	3.2	8.0	0.8	20	nd	2
Heptanal	0.9	3.4	0.9	10	nd	2
Octanal	3.2	15.3	1.0	20	nd	2
Nonanal	9.8	85.5	1.1	20	nd	2
Decanal	4.0	9.1	1.0	20	nd	2
1-Octanol	bdl	3.8	bdl	nd	nd	nd
1-Nonanol	bdl	3.4	bdl	nd	nd	nd
Butanoic acid, 3-methyl-	1.1	0.6	0.2	nd	nd	nd
Pentanoic acid	1.0	0.1	0.1	30	10	3
Benzoic acid	2.7	0.2	0.1	nd	nd	nd
S_6, S_7, S_8	1.6	0.2	bdl	nd	nd	nd

Q-B quartz-barite heap, *B-P* barit-pyrite heap, *BG* background values, *msd* maximal single dose, *ad* average daily, *hc* hazard class, *n.d.* no data

found (compared to all detected organic gases): 31 and 43.4 μg/m^3, respectively. It should be noted that carbon disulfide is a volatile compound of the second hazard class, its average daily maximum allowable concentration in the air of populated areas is 5 μg/m^3, the maximum single dose is 30 μg/m^3 according to the hygienic standards adopted in the Russian Federation (RMH 2003) that is, the found concentrations exceed 6–8 times the daily average norm and even higher than the maximum one-time. Considering that the studied heaps are located in the territory of the Ursk village, further monitoring of the concentrations of this compound in the field deserves special attention and will be the subject of study in our further studies in this area and other similar objects.

The dimethyl selenide (C_2H_6Se) was detected over the pyrite heap in the concentration of 51.8 μg/m^3. We explain its formation by microbiological methylation of selenium-containing compounds, which we also wrote earlier (Bortnikova et al. 2019). In addition, we first discovered formamides, aromatic and heterocyclic compounds (Table 3), quantitative estimates were given for their concentrations.

Methylated forms of formamide, N, N-dimethyl- and formamide, N-formyl-N-methyl-formamides are found in concentrations of 75 and 6.5 ppb, respectively (Table 3). Formamide, N, N-dimethyl- is the third in the level of concentrations among all organosulfur gases in the air above the pyrite dump (after C_2H_6Se and CS_2). Probably, both compounds are also participants of the

same biotic cycle with methylation, which we wrote about above. In addition, it is interesting that formamides are intermediates in the methanogenesis cycle and can be the source of the highly toxic hydrogen cyanide (HCN) (Bipp and Kieczka 2012).

It is also known that formamide is a safe product of enzymatic conversion of toxic cyanide, for example, phytopathogenic fungi using cyanide hydratase by reaction (Mansfield 2000; Gupta et al. 2010):

$$HCN + H_2O \rightarrow HCONH_2.$$

In addition to detoxifying of cyanide, a number of fungi carry out the reaction of converting cyanide to formamide in order to use cyanide as a source of nitrogen. Pereira et al. (1996) identified three fungi from industrial effluents that grew on cyanide as the only source of nitrogen: F. oxisporum, Trichoderma koningii, and Gliocladium virens.

Since the wastes we study are formed as a result of sulfide-containing ores cyanidation, it can be assumed that a number of nitrogen-containing compounds found in the air above the dumps, for example, the aforementioned formamide derivatives, are products of the biotic conversion of cyanides and rodanides. Further study of the nitrogen-containing gases seasonal dynamics over the Ursk waste heaps can provide information on the intensity of cyanidation waste biodegradation, depending on the season, which is an urgent task in the conditions of the Siberian climate.

In addition, aromatic compounds are detected over quartz-barite dumps: benzamide, N, N-dimethyl- (6 μg/m^3), phenol (3 μg/m^3), benzonitrile, C_6H_5CN (17.2 μg/m^3), benzyl nitrile, C_7H_7CN (0.4 μg/m^3), benzenepropanenitrile C_8H_9CN (0.2 μg/m^3). As for the above-described nitriles (C_6H_5CN, C_7H_7CN, C_8H_9CN), they are derived from hydrocyanic acid. Their formation may be associated with the transformation of cyanide residues that are part of the waste. Nitriles are poisonous to humans due to the disruption of the action of cytochrome oxidase and the inhibition of the function of oxygen transfer from the blood to the cells. The toxic effect is manifested both by inhalation of nitrile vapors and by ingestion through the skin or the gastrointestinal tract. Unconditional interest is caused by the mechanisms of formation of such compounds, seasonal variations in their concentrations, localization of the most active breathing zones, their relationship with environmental parameters.

In this paper, we combine geophysical and geochemical methods to obtain a general picture of the distribution of chemical compounds in a solid-pore solution-atmosphere system; we make judgments about the mobility of chemical elements and organic compounds during the hypergene transformation of a technogenic system.

It was shown that the areas subject to the greatest hypergene changes are detected with the help of electrotomography as areas of anomalous resistance, these same zones are characterized by increased gas evolution. Among these gases, there is a whole spectrum, including hazardous organic gases, whose concentrations are higher than the maximum permissible, but their origin in these dumps is not completely clear and requires further research. In addition, the toxicity of a number of gases has not been studied at all, toxicological tests are necessary, the relevance of which is beyond doubt due to the fact that the studied and similar wastes are located next to residential areas.

5 Conclusions

1. A study of the composition of gases in the surface part of the heaps was conducted by the example of two heaps with the contrasting composition of the tailings and different degrees of oxidation of the tailings.
2. The intensity of gas emanations depend on the external environmental conditions, in particular, on fluctuations in air and ground temperatures. The highest gas concentrations were found in areas with anomalous temperature and the presence of channels of infiltration of pore solutions to the surface. The most intensive geochemical transformations are subjected to a layer of seasonal temperature fluctuations, in which chemical leaching is activated, associated with rock cracking under the influence of expanding and freezing pore fluid. The sulfide-bearing rock is exposed in such conditions the oxidation in summer and methylation in winter.
3. Sulfide-containing heaps are a source of anomalous concentrations of sulfur- and nitrogen containing gases in the air: DMS, DMSO, CS_2, SO_2, methylated forms of formamide, N, N-dimethyl- and Formamide, N-formyl-N-methyl-formamides. The intake and concentration of gases are determined by the internal structure of the heaps and the degree

of oxidation of the tailings. The presence of highly conductive zones (the presence of highly mineralized solutions) in the surface parts of the heaps leads to the intensive production of the gases. In areas with high resistivity (relatively "dry" areas) the intake of gases into the air is lower by an order of magnitude. The oxidized quartz-barite heap and profile along the debris cone is characterized by a higher concentration of gases than the pyrite-barite (less oxidized) heap.

Acknowledgments The authors are grateful to the Assistant Editors for the editorial handling of the manuscript.

Compliance with Ethical Standards

Funding This research was funded by the Russian Science Foundation [19-17-00134].

References

Auken, E., Doetsch, J., Fiandaca, G., Christiansen, A. V., Gazoty, A., Cahill, A. G., & Jakobsen, R. (2014). Imaging subsurface migration of dissolved CO_2 in a shallow aquifer using 3-D time-lapse electrical resistivity tomography. *Journal of Applied Geophysics, 101*, 31–41. https://doi.org/10.1016/j.jappgeo.2013.11.011.

Bates, T. S., Lamb, B. K., Guenther, A., Dignon, J., & Stoiber, R. E. (1992). Sulfur emissions to the atmosphere from natural sources. *Journal of Atmospheric Chemistry, 14*, 315–337. https://doi.org/10.1007/BF00115242.

Beloborodova, N. V., & Beloborodov, S. M. (2000). Metabolites of anaerobic bacteria (volatile fatty acids) and reactivity of the microorganism. *Antibiotics and Chemotherapy, 2*, 28–36.

Bergmann, P., Schmidt-Hattenberger, C., Labitzke, T., Wagner, F. M., Just, A., Flechsig, C., & Rippe, D. (2017). Fluid injection monitoring using electrical resistivity tomography-five years of CO_2 injection at Ketzin, Germany. *Geophysical Prospecting, 65*(3), 859–875. https://doi.org/10.1111/1365-2478.12426.

Binley, A., Hubbard, S. S., Huisman, J. A., Revil, A., Robinson, D. A., Singha, K., & Slater, L. D. (2015). The emergence of hydrogeophysics for improved understanding of subsurface processes over multiple scales. *Water Resources Research, 51*(6), 3837–3866. https://doi.org/10.1002/2015WR017016.

Bipp, H., & Kieczka, H. (2012). Formamides, Ullmann's Encyclopedia of Industrial Chemistry. *Weinheim: Wiley-VCH*. https://doi.org/10.1002/14356007.a12_001.pub2.

Bolgov GP (1937) Salaire sulfides, Ursk group of polymetallic deposits Izv. Tomsk. Polytechnic Inst., №53 (11), p. 45-96 (in Russian)

Bortnikova, S., Olenchenko, V., Gaskova, O., Chernii, K., Devyatova, A., & Kucher, D. (2017). Evidence of trace element emission during the combustion of sulfide-bearing metallurgical slags. *Applied Geochemistry, 78*, 105–115. https://doi.org/10.1016/j.apgeochem.2016.12.016.

Bortnikova, S. B., Yurkevich, N. V., Abrosimova, N. A., Devyatova, A. Y., Edelev, A. V., Makas, A. L., & Troshkov, M. L. (2018). Assessment of emissions of trace elements and sulfur gases from sulfide tailings. *Journal of Geochemical Exploration, 186*, 256–269. https://doi.org/10.1016/j.gexplo.2017.12.008.

Bortnikova, S., Yurkevich, N., Devyatova, A., Saeva, O., Shuvaeva, O., Makas, A., Troshkov, M., Abrosimova, N., Kirillov, M., Korneeva, T., & Kremleva, T. (2019). Mechanisms of low-temperature vapor-gas streams formation from sulfide mine waste. *Science of the Total Environment, 647*, 411–419. https://doi.org/10.1016/j.scitotenv.2018.08.024.

Bowman, J. H., Barket, D. J., & Shepson, P. B. (2003). Atmospheric chemistry of nonanal. *Environmental Science and Technology, 37*(10), 2218–2225. https://doi.org/10.1021/es026220p.

Brimblecombe, P. (2013). The global sulfur cycle. In K. Turekian & H. Holland (Eds.), *Treatise on Geochemistry* (pp. 559–591). Elsevier Inc.. https://doi.org/10.1016/B0-08-043751-6/08134-2.

BS ISO. (1998). *Soil quality - determination of the water-retention characteristic*. Geneva: BS ISO.

Busato, L., Boaga, J., Perri, M. T., Majone, B., Bellin, A., & Cassiani, G. (2019). Hydrogeophysical characterization and monitoring of the hyporheic and riparian zones: The Vermigliana Creek case study. *Science of the Total Environment, 648*, 1105–1120. https://doi.org/10.1016/j.scitotenv.2018.08.179.

Cahill, A. G., Steelman, C. M., Forde, O., Kuloyo, O., Ruff, S. E., Mayer, B., Mayer, K. U., Strous, M., Ryan, M. C., Cherry, J. A., & Parker, B. L. (2017). Mobility and persistence of methane in groundwater in a controlled-release field experiment. *Nature Geoscience, 10*(4), 289. https://doi.org/10.1038/ngeo2919.

Carrión, O., Pratscher, J., Curson, A. R. J., Williams, B. T., Rostant, W. G., Murrell, J. C., & Todd, J. D. (2017). Methanethiol-dependent dimethylsulfide production in soil environments. *The ISME Journal, 11*, 2379–2390. https://doi.org/10.1038/ismej.2017.105.

Charlson, R. J., Lovelock, J. E., Andreae, M. O., & Warren, S. G. (1987). Oceanic phytoplankton, atmospheric Sulphur, cloud albedo and climate. *Nature, 326*, 655–661. https://doi.org/10.1038/326655a0.

Distanov, E.G., 1977. Pyrite-Polymetallic Deposits of Siberia [in Russian]. Nauka, Novosibirsk.

Epov, M. I., Yurkevich, N. V., Bortnikova, S. B., Karin, Y. G., & Saeva, O. P. (2017). Analysis of mine waste by geocheimical and geophysical methods (a case study of the mine tailing dump of the Salair ore-processing plant). *Russian Geology and Geophysics, 58*(12), 1543–1552. https://doi.org/10.1016/j.rgg.2017.11.014.

GN (Hygienic Norms) no. 2.1.6.1338–03. (2003). Maximum permissible concentration of chemical pollutants in the atmospheric air populations. *M.: Ministry of Health of the Russia.*

Golebiowski, T., Zogala, B., Mendecki, M. J., & Malysa, T. (2018). The utility of rock-bolts as long electrodes for underground ERT surveys in mine settings. *Journal of Applied Geophysics, 155*, 122–130. https://doi.org/10.1016/j.jappgeo.2018.05.010.

Gourdal, M., Lizotte, M., Massé, G., Gosselin, M., Poulin, M., Scarratt, M., Charette, J., & Levasseur, M. (2018). Dimethyl sulfide dynamics in first-year sea ice melt ponds in the Canadian Arctic archipelago. *Biogeosciences, 15*(10), 3169–3188. https://doi.org/10.5194/bg-15-3169-2018.

Guérin, R. (2005). Borehole and surface-based hydrogeophysics. *Hydrogeology Journal, 13*(1), 251–254. https://doi.org/10.1007/s10040-004-0415-4.

Gupta, N., Balomajumder, C., & Agarwal, V. K. (2010). Enzymatic mechanism and biochemistry for cyanide degradation: A review. *Journal of Hazardous Materials, 176*(1–3), 1–13. https://doi.org/10.1016/j.jhazmat.2009.11.038.

Hale, M. (1993). Mineral deposits and chalcogen gases. *Mineralogical Magazine, 57*, 599–606. https://doi.org/10.1180/minmag.1993.057.389.04.

Hale, M. (2010). Gas geochemistry and deeply buried mineral deposits: The contribution of the applied geochemistry research group, Imperial College of Science and Technology, London. *Geochemistry Exploration Environment Analysis, 10*, 261–267. https://doi.org/10.1144/1467-7873/09-236.

Hayes, A. C., Liss, S. N., & Allen, D. G. (2010). Growth kinetics of Hyphomicrobium and Thiobacillus spp. in mixed cultures degrading dimethyl sulfide and methanol. *Applied and Environmental Microbiology, 76*, 5423–5431. https://doi.org/10.1128/AEM.00076-10.

Johnson, S. D., & Jürgens, A. (2010). Convergent evolution of carrion and faecal scent mimicry in fly-pollinated angiosperm flowers and a stinkhorn fungus. *South African Journal of Botany, 76*(4), 796–807. https://doi.org/10.1016/j.sajb.2010.07.012.

Jougnot, D., Jiménez-Martínez, J., Legendre, R., Le Borgne, T., Méheust, Y., & Linde, N. (2018). Impact of small-scale saline tracer heterogeneity on electrical resistivity monitoring in fully and partially saturated porous media: Insights from geoelectrical milli-fluidic experiments. *Advances in Water Resources, 113*, 295–309. https://doi.org/10.1016/j.advwatres.2018.01.014.

Kiene, R. P. (1990). Dimethyl sulfide production from dimethylsulfoniopropionate in coastal seawater samples and bacterial cultures. *Applied and Environmental Microbiology, 56*, 3292–3297.

Kiene, R. P., Linn, L. J., & Bruton, J. A. (2000). New and important roles for DMSP in marine microbial communities. *Journal of Sea Research, 43*(3–4), 209–224. https://doi.org/10.1016/S1385-1101(00)00023-X.

Koch, T., & Dahl, C. (2018). A novel bacterial sulfur oxidation pathway provides a new link between the cycles of organic and inorganic sulfur compounds. *The ISME Journal, 12*, 2479–2491. https://doi.org/10.1038/s41396-018-0209-7.

Kovalev KR (1969) Features of the formation of ores of pyrite-polymetallic deposits of the North-Eastern Salair and East Tuva // Candidate's dissertation of geol. mineral. sciences. Novosibirsk, 32 p (in Russian)

Kremer, T., Vieira, C., & Maineult, A. (2018). ERT monitoring of gas injection into water saturated sands: Modeling and inversion of cross-hole laboratory data. *Journal of Applied Geophysics, 158*, 11–28. https://doi.org/10.1016/j.jappgeo.2018.06.001.

Kruszewski, Ł., Fabiańska, M. J., Ciesielczuk, J., Segit, T., Orłowski, R., Motyliński, R., Kusy, D., & Moszumańska, I. (2018). First multi-tool exploration of a gas-condensate-pyrolysate system from the environment of burning coal mine heaps: An in situ FTIR and laboratory GC and PXRD study based on upper Silesian materials. *Science of the Total Environment, 640*, 1044–1071. https://doi.org/10.1016/j.scitotenv.2018.05.319.

Lazareva, E. V., Myagkaya, I. N., Kirichenko, I. S., Gustaytis, M. A., & Zhmodik, S. M. (2019). Interaction of natural organic matter with acid mine drainage: In-situ accumulation of elements. *Science of the Total Environment, 660*, 468–483. https://doi.org/10.1016/j.scitotenv.2018.12.467.

Ledyard, K. M., & Dacey, J. W. H. (1996). Microbial cycling of DMSP and DMS in coastal and oligotrophic seawater. *Limnology and Oceanography, 41*, 33–40. https://doi.org/10.4319/lo.1996.41.1.0033.

Lee, P. A., & de Mora, S. J. (1999). Intracellular dimethylsulfoxide (DMSO) in unicellular marine algae: Speculations on itsorigin and possible biological role. *Journal of Phycology, 35*, 8–18. https://doi.org/10.1046/j.1529-8817.1999.3510008.x.

Loke, M. H. (2000). *Electrical imaging surveys for environmental and engineering studies, a practical guide to 2D and 3D surveys*. Malaysia: Penang.

Makas, A. L., & Troshkov, M. L. (2004). Field gas chromatography – Mass spectrometry for fast analysis. *Journal of Chromatography, B, 800*(1–2), 55–61. https://doi.org/10.1016/j.jchromb.2003.08.054.

Malin, G., & Kirst, G. O. (1997). Algal production of dimethyl sulfide and its atmospheric role. *Journal of Phycology, 33*, 889–896. https://doi.org/10.1111/j.0022-3646.1997.00889.x.

Mansfield, J. W. (2000). Antimicrobial compounds and resistance: The role of phytoalexins and phytoanticipins. In A. J. Slusarenko, R. S. S. Fraser, & L. C. van Loon (Eds.), *Mechanisms of resistance to plant diseases* (pp. 325–370). Dodrecht: Kluwer Academic Publishers.

Meng, T., Zhu, T., Zhang, J., & Cai, Z. (2015). Effect of liming on sulfate transformation and sulfur gas emissions in degraded vegetable soil treated by reductive soil disinfestation. *Journal of Environmental Sciences, 36*, 112–120. https://doi.org/10.1016/j.jes.2015.03.032.

Nicholson, R. A., Peachey, D., & Ball, T. K. (1988). Tests on use of Sulphur gases in soils to detect hidden mineralization. *Transactions of the Institution of Mining and Metallurgy, 971*, B57–B63.

Olenchenko, V. V., Kucher, D. O., Bortnikova, S. B., Gas'kova, O. L., Edelev, A. V., & Gora, M. P. (2016). Vertical and lateral spreading of highly mineralized acid drainage solutions (Ur dump, Salair): Electrical resistivity tomography and hydrogeochemical data. *Russian Geology and Geophysics, 57*(4), 617–628. https://doi.org/10.1016/j.rgg.2015.05.014.

Osipova, P. S., Olenchenko, V. V., Bortnikova, S. B., & Yurkevich, N. V. (2018). Dependence of the electrical resistivity of mine tailings from the daily temperature dynamics. *Interexpo GEO-Siberia, 2*(4), 68–74. https://doi.org/10.18303/2618-981X-2018-4-68-74.

Pereira, P. T., Arrabaça, J. D., & Amaral-Collaço, M. T. (1996). Isolation, selection and characterization of a cyanide-

degrading fungus from an industrial effluent. *International Biodeterioration & Biodegradation, 37*(1–2), 45–52. https://doi.org/10.1016/0964-8305(95)00086-0.

Pticyn, A. B. (2006). *Teoreticheskaja geohimija*. Novosibirsk: Akademicheskoe izdatel'stvo Geo.

RMH. (2003). *Maximum permissible concentration (MPC) of pollutants in the atmospheric air of populated areas HN 2.1.6.1338–03, 2003*. Moscow: Russian Ministry of Health.

Simó, R. (2001). Production of atmospheric sulfur by oceanic plankton: Biogeochemical, ecological and evolutionary links. *Trends in Ecology and Evolution, 16*, 287–294. https://doi.org/10.1016/S0169-5347(01)02152-8.

Statheropoulosa, M., Agapioua, A., Spiliopoulou, C., Pallis, G. C., & Sianos, E. (2007). Environmental aspects of VOCs evolved in the early stages of human decomposition. *Science of the Total Environment, 385*(1–3), 221–227. https://doi.org/10.1016/j.scitotenv.2007.07.003.

Steelman, C. M., Klazinga, D. R., Cahill, A. G., Endres, A. L., & Parker, B. L. (2017). Monitoring the evolution and migration of a methane gas plume in an unconfined sandy aquifer using time-lapse GPR and ERT. *Journal of Contaminant Hydrology, 205*, 12–24. https://doi.org/10.1016/j.jconhyd.2017.08.011.

Stensmyr, M. C., Urru, I., Collu, I. U., Celander, M., Hansson, B. S., & Angioy, A.-M. (2002). Rotting smell of dead-horse arum florets. Nature, 420(6916), 625–626. https://doi.org/10.1038/420625.

Sunda, W., Kieber, D. J., Kiene, R. P., & Huntsman, S. (2002). An an-tioxidant function for DMSP and DMS in marine algae. *Nature, 418*, 317–320. https://doi.org/10.1038/nature00851.

Terry, N., Slater, L., Comas, X., Reeve, A. S., Schäfer, K. V., & Yu, Z. (2016). Free phase gas processes in a northern peatland inferred from autonomous field-scale resistivity imaging. *Water Resources Research, 52*(4), 2996–3018. https://doi.org/10.1002/2015WR018111.

Vila-Costa, M., Simó, R., Harada, H., Gasol, J. M., Slezak, D., & Kiene, R. P. (2006). Dimethylsulfoniopropionate uptake by marine phytoplankton. *Science, 314*, 652–654. https://doi.org/10.1126/science.1131043.

Xue, Z., Tanase, D., & Watanabe, J. (2006). Estimation of CO_2 saturation from time-lapse CO_2 well logging in an onshore aquifer, Nagaoka, Japan. *Exploration Geophysics, 37*, 19–29. https://doi.org/10.1071/EG06019.

Yurkevich, N., Bortnikova, S., Olenchenko, V., Abrosimova, N., Saeva, O., & Karin, Y. (2017a). Study of water-rock interaction in sulfide mining tailings using geochemical and geoelectrical methods. *Procedia Earth and Planetary Science, 17*, 112–115. https://doi.org/10.1016/j.proeps.2016.12.019.

Yurkevich, N. V., Abrosimova, N. A., Bortnikova, S. B., Karin, Y. G., & Saeva, O. P. (2017b). Geophysical investigations for evaluation of environmental pollution in a mine tailings area. *Toxicological and Environment Chemistry, 99*, 1328–1345. https://doi.org/10.1080/02772248.2017.1371308.

Zerkalov, V. I. "New minerals in ores of the Ur deposits, Salair." Vestnik (1959).

Publisher's Note Springer Nature remains neutral with regard to jurisdictional claims in published maps and institutional affiliations.